Band-edge biexciton in nanocrystals of semiconductors with a degenerate valence band

A. V. Rodina
A. F. Ioffe Physico-Technical Institute, 194021 St.-Petersburg, Russia

Al. L. Efros
Naval Research Laboratory, Center for Computational Material Science, Washington, DC 20375, USA
(Received 15 July 2010; published 24 September 2010)

We present a theoretical analyses of the fine structure of the band-edge biexciton in nanometer-size crystallites [nanocrystal (NC) quantum dots] of direct semiconductors with a cubic lattice structure or a hexagonal lattice structure, which can be described within the framework of a quasicubic lattice model. The six ground biexciton states created from the two fourfold degenerate hole states and the two twofold degenerate electron states, according to the Pauli principle, are split into three levels by the crystal-shape asymmetry, the intrinsic crystal field (in hexagonal lattice structure), and the hole-hole exchange interaction. The size-dependent splitting and oscillator transition strength between the biexciton states and the ground exciton states were calculated in NCs with different types of spatial confinement: NCs surrounded by impenetrable barrier and NCs with a soft confinement created by gradually changing along the radius composition of the alloy forming the NC. The results of the calculations were compared with available experimental data on CdSe NCs.

DOI: 10.1103/PhysRevB.82.125324 PACS number(s): 73.22.−f, 78.67.Bf

I. INTRODUCTION

One of the properties possessed by nanocrystal (NC) assemblies that are most important for future applications is their strong nonlinear optical response.[1,2] Nonlinear optical effects in absorption can be observed at relatively low excitation power because a second electron hole pair in a NC is excited in the presence of the electric field of the first pair, which affects the transition energy and oscillator strength of the second.[3–5] The energy spectra of two electron-hole (e-h) pairs created from ground electron and hole states or the ground biexciton state are especially important because they determine almost all the band-edge nonlinear optical properties of NCs including stimulated emission.[6] This is a unique property of strongly confined NC quantum dots. In the NCs, the ground electron state is a $1S_e$ level, which is twofold degenerate with respect to the spin projection.[7] It is separated from the next $1P_e$ level, typically by 200–300 meV.[8] The Pauli principle allows only two electrons to occupy the first $1S_e$ level and excitation of the third e-h pair requires an extra 200–300 meV. Thus, the band-edge nonlinear optical properties of NCs are determined *only* by the optically allowed transitions between single exciton states and two e-h pair states, i.e., band-edge biexciton states. These states also participate directly in various types of pump-probe experiments conducted in NCs, such as pump-probe Faraday rotation, for example.[9]

Despite the important role biexcitons play in the optics of NCs, it has been practically impossible to observe the biexciton line in the photoluminescence (PL) of the NCs under steady-state excitation conditions. The radiative decay time of biexcitons in NCs is on the order of several nanoseconds and is much longer than their nonradiative Auger recombination time, which was measured to be 10–300 ps, depending on NC size.[10] As a result, the nonradiative Auger recombination completely quenches the steady-state PL in NCs. The biexciton lines were observed only in a stimulated emission from the biexciton confined in the NC because the stimulated emission time could be shorter than nonradiative Auger recombination,[6] and in the transient absorption[11–13] or transient PL experiments.[14–16] These experiments have measured the binding energy of the ground biexciton state.

Recently, the fine structure of the optical transitions between band-edge biexciton and exciton states and vice versa was partially resolved in transient absorption and PL experiments conducted on CdSe NCs.[17] These experiments showed a significant difference in biexciton binding energies measured in absorption and PL, which was attributed to the fine structure of the band-edge exciton. The first-principles calculation of the fine structure conducted in Ref. 17 reproduce, however, the experimental observations only qualitatively. This may be connected with the fact that the wave functions of two holes creating a biexciton was not properly antisymmetrized in Ref. 17. The antisymmetrization of the holes from the Γ_8 valence subband leads to the hole exchange splitting of the ground biexciton state into two biexciton states even in spherical NCs, namely, the ground fivefold degenerate state with total angular momentum $\boldsymbol{J}=2$ and the excited state with $\boldsymbol{J}=0$.[18] More generally, the hole-hole (h-h) exchange interaction leads to a nonequidistant biexciton level structure, instead of the equidistant one calculated in Ref. 17, and it modifies the optical selection rules.

One also could expect direct measurements of the biexciton fine structure in steady-state PL experiments. Such measurements became feasible recently because a new generation of NCs with a suppressed rate of nonradiative Auger processes was reported by several groups.[19–22] The suppression was connected with softening of the confinement potential (CP) created by the gradual variation of the alloy composition along the NC radius[19] or by interfacial diffusion in core/shell NCs.[21] The direct biexciton PL under steady-state excitation conditions was already reported in single NC measurements.[22]

In this paper we present realistic multiband calculations of the band-edge biexciton fine structures in NCs of semiconductors having a degenerate valence band, which takes into

account the effect of h-h exchange interaction, nonsphericity of the NC shape, and the intrinsic hexagonal lattice symmetry. Using the obtained spectra we discuss the optical selection rules and calculate the oscillator transition strength for optically allowed transitions between band-edge biexciton and exciton states and vice versa. The general theory is applied to NCs with abrupt confinement and to NCs whose confinement is created by radial variation of the chemical composition. The theoretical results are compared with available experimental data.

The paper is organized as follows: In Sec. II we present general expressions that describe the fine structure of the band-edge biexciton in a semiconductor with a degenerate valence band and the transition matrix elements for optically allowed transitions between levels of the band-edge exciton and the band-edge biexciton. In Sec. III we calculate the size dependence of the biexciton energy spectra and optically allowed transition probabilities for several semiconductor NCs with soft and abrupt confinement. The discussion of the obtained results and their comparison with available experimental data are given in Sec. IV.

II. FINE STRUCTURE OF BAND-EDGE BIEXCITON

In this paper we consider almost spherical NCs of direct-gap semiconductors with a cubic lattice structure or a hexagonal lattice structure, which can be described within the framework of a quasicubic lattice model. The radius of considered NCs, a, is supposed to be sufficiently small to allow us to use the strong confinement approximation[7] and to consider all Coulomb interactions between electrons and holes perturbatively.[23] In NCs of such size, the energy spectra and wave functions of excitons and biexcitons are determined by the energy spectra of independent electrons and holes in the first approximation.

The biexciton spectra will be studied for two types of carrier confinement in NCs. The first one considers the NC surface as an impenetrable barrier. This approach successfully describes the energy spectra of electrons and holes and the fine structure of the band-edge excitons in bare CdSe NCs in Refs. 8 and 24–27, respectively. The second one describes NCs with soft confinement potential (SCNCs). This soft CP is created, for example, in alloyed semiconductor compound, $A_xB_{1-x}C$, whose composition, x, changes gradually along the NC radius from $x=0$ at the NC center to $x=1$ at the NC surface.[19] We will model the CP in these SCNCs by a parabolic potential assuming that electrons and holes are localized at the NC center. For numerical modeling of the biexciton energy spectra in the SCNCs the curvature of the parabolic potentials will be calculated from the band offsets between bulk AC and BC compounds for electrons and holes, respectively. In the following discussion we will generalize the expressions for the fine structure of exciton energy spectra described in Ref. 25 that would allow one to use them in any type of CP and still keep the notations introduced in Refs. 25–27.

A. Band-edge levels of electrons and holes

Let us describe briefly a structure of the lowest quantum size levels in a spherical NC. The electron ground state in the conduction band is a spherically symmetrical $1S_e$ state that is twofold degenerate with respect to the spin projection. The wave function of the state could be written

$$\Psi_\alpha^e(\boldsymbol{r}) = \xi(\boldsymbol{r})|S\alpha\rangle = R_e(r)Y_{00}(\Omega)|S\alpha\rangle, \tag{1}$$

where $|S\alpha\rangle$ are the Bloch functions of the conduction band, and $\alpha=\uparrow$ $(\downarrow)$ is the projection of the electron spin, $s_z=+(-)1/2$. The spherical harmonic function, $Y_{lm}(\Omega)$, for the $1S_e$ level has both $l=0$ and $m=0$. The radial component of the electron wave function, $R_e(r)$, in the parabolic band approximation satisfies the standard equation

$$-\frac{\hbar^2}{2m_e}\left(\frac{\partial}{\partial r}+\frac{2}{r}\right)\frac{\partial}{\partial r}R_e(r)+[V_e(r)-E_{1S}]R_e(r)=0, \tag{2}$$

where $V_e(r)$ is the potential that confines the electron motion in a NC and m_e is the electron effective mass. Equation (2) should be accompanied by some boundary condition at the NC surface at $r=a$. In NCs surrounded by an impenetrable barrier the standard boundary condition leads to the radial function, $R_e^{\mathrm{SBC}}(r)$, which may be found, e.g., in Ref. 28. We will refer to such confinement as the "standard CP for electrons" throughout the paper.

In this paper we also consider electrons confined in the parabolic spherical potential $V_e(r)=k_cr^2/2=(m_e\omega_e^2r^2)/2$, where k_c is the spring constant of the potential defining the electron characteristic frequency ω_e. The ground energy level, E_{1S}, and the radial function can be written

$$E_{1S}=\frac{3}{2}\hbar\omega_e=\frac{3\hbar^2}{2m_eL_e^2},\quad R_e(r)=\frac{2}{\pi^{1/4}L_e^{3/2}}\exp\left(-\frac{r^2}{2L_e^2}\right), \tag{3}$$

where $L_e=\sqrt{\hbar/(m_e\omega_e)}$ is the electron oscillator length characterizing the electron localization at the NC center. In our calculations, we connect the parabolic potential spring constant k_c in alloyed $A_xB_{1-x}C$ NCs with the conduction band offset between bulk AC and BC pure compound semiconductors, V_e^{off}, assuming that $x=1$ at the NC surface and $x=0$ at the NC center. This results in $L_e^2=a\sqrt{\hbar^2/(2m_eV_e^{off})}$, which characterizes completely the electron ground state in this parabolic CP.

The first quantum-size level of holes in a spherical NC of a semiconductor with a degenerate Γ_8 valence subband is a $1S_{3/2}$ state.[8] This state has total angular momentum $\boldsymbol{j}=3/2$ and is fourfold degenerate with respect to its projection $M=3/2,1/2,-1/2,-3/2$ on the z axis.[8,29] The wave functions of this state could be written[30]

$$\Psi_M^h=2\sum_{l=0,2}(-1)^{l-3/2+M}R_l(r)\sum_{m+\mu=M}\begin{pmatrix} l & 3/2 & 3/2 \\ m & \mu & -M \end{pmatrix}Y_{l,m}u_\mu, \tag{4}$$

where $\begin{pmatrix} i & k & l \\ m & n & p \end{pmatrix}$ are the Wigner $3j$ symbols, and u_μ $(\mu=\pm1/2,\pm3/2)$ are the Bloch functions of the fourfold degenerate valence band Γ_8 (Ref. 31)

$$u_{3/2}=\frac{1}{\sqrt{2}}(X+iY)\uparrow,\quad u_{-3/2}=\frac{i}{\sqrt{2}}(X-iY)\downarrow,$$

$$u_{1/2} = \frac{i}{\sqrt{6}}[(X+iY)\downarrow - 2Z\uparrow],$$

$$u_{-1/2} = \frac{1}{\sqrt{6}}[(X-iY)\uparrow + 2Z\downarrow]. \quad (5)$$

The radial wave functions R_0 and R_2 in Eq. (4) are normalized: $\int(R_0^2+R_2^2)r^2dr=1$ and satisfy the following system of radial equations:[32,33]

$$(1+\beta)\hat{A}_1^-\hat{A}_0^+R_0(r) + (1-\beta)\hat{A}_1^-\hat{A}_2^-R_2(r) = \frac{2m_h}{\hbar^2}[E_{1S_{3/2}} - V_h(r)]R_0(r),$$

$$(1-\beta)\hat{A}_1^+\hat{A}_0^+R_0(r) + (1+\beta)\hat{A}_1^-\hat{A}_2^-R_2(r) = \frac{2m_h}{\hbar^2}[E_{1S_{3/2}} - V_h(r)]R_2(r), \quad (6)$$

where $\beta=m_l/m_h$ is the ratio of light to heavy hole effective masses: m_l and m_h, respectively, $V_h(r)$ is the potential that confines the hole motion in a NC and the differential operators $\hat{A}_l^+$ and $\hat{A}_l^-$ are defined as

$$\hat{A}_l^+ = -\frac{\partial}{\partial r} + \frac{l}{r}, \quad \hat{A}_l^- = \frac{\partial}{\partial r} + \frac{l+1}{r}. \quad (7)$$

To find the energy, $E_{1S_{3/2}}$, and the radial functions of the ground state, one must accompany Eq. (6) by some boundary condition at the NC surface at $r=a$. In NCs surrounded by an impenetrable barrier, the standard boundary condition leads to the radial functions, $R_0^{\mathrm{SBC}}(r)$ and $R_2^{\mathrm{SBC}}(r)$, which could be found, for example, in Refs. 25 and 34. We will refer to such confinement as the standard CP for holes throughout the paper.

In this paper we also consider holes in a parabolic confinement potential: $V_h(r)=k_v r^2/2 \equiv (m_h\omega_h^2 r^2)/2$. Here the spring constant k_v of the parabolic potential in alloyed $A_xB_{1-x}C$ NCs is connected with the valence band offset between bulk AC and BC pure compound semiconductors, $V_h^{off}=V_h(a)$, and defines the typical frequency of the heavy hole motion, ω_h. To find the hole ground state level $E_{1S_{3/2}}$ we use the variational approach.

The form of selected variational functions allows them to transfer into the functions satisfying Eqs. (6) for the two limiting cases $\beta=1$ and $\beta=0$. For the case of $\beta=1$ the system of Eq. (6) describes two, twofold degenerate particles that are moving in parabolic confinement potential. The radial dependence of the hole wave functions in this case have a standard Gaussian form similar to the electron radial function in Eq. (3). Although the exact solution of Eq. (6) for $\beta=0$ is not known, the radial functions R_0 and R_2, however, must satisfy the exact differential condition[18]

$$\frac{dR_0}{dr} + \frac{dR_2}{dr} + \frac{3}{r}R_2 = 0. \quad (8)$$

These selection principles lead to the following variational function:

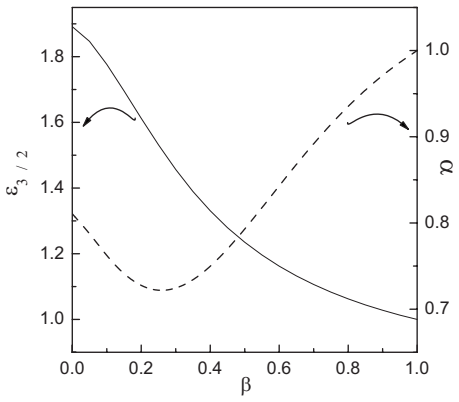

FIG. 1. Dimensionless ground-state energy $\varepsilon_{3/2}$ of the hole confined in spherical parabolic potential (solid line) and the respective variational parameter α (dashed line) as a function of the ratio of the light to heavy-hole effective masses, β.

$$R_2(r) = C\frac{\alpha r^2}{2L_h^2}\left[\exp\left(-\frac{\alpha r^2}{2L_h^2}\right) - \beta^2\exp\left(-\frac{\alpha r^2}{2L_l^2}\right)\right], \quad (9)$$

$$R_0(r) = C\frac{3}{2}\left[\exp\left(-\frac{\alpha r^2}{2L_h^2}\right) + \beta^{3/2}\exp\left(-\frac{\alpha r^2}{2L_l^2}\right)\right] - R_2(r), \quad (10)$$

where α is the variational parameter, $L_h=\sqrt{\hbar/(k_v m_h)^{1/2}} \equiv \sqrt{\hbar/m_h\omega_h}$ and $L_l=\sqrt{\hbar/(k_v m_l)^{1/2}}=L_h/\beta^{1/4}$ are the oscillator length of the heavy and light holes, respectively, and C is the normalization constant. The variational procedure gives for the ground-state energy

$$E_{1S_{3/2}}(\beta) = \frac{3}{2}\hbar\omega_h\epsilon_{3/2}(\beta) = \frac{3}{2}\frac{\hbar^2}{m_h L_h^2}\epsilon_{3/2}(\beta). \quad (11)$$

The dimensionless function $\epsilon_{3/2}(\beta)$ is plotted in Fig. 1. Its value decreases from $\sqrt{161/45}$ to 1 while β increases from 0 to 1. The variational parameter $\alpha(\beta)$ is also plotted in Fig. 1 and it changes with β from $\sqrt{23/35}$ to 1. In our calculation, L_h is related to the NC radius a as $L_h^2=a\sqrt{\hbar^2/(2m_h V_h^{off})}$ and characterizes completely the ground state of holes in the parabolic CP.

Nanocrystal asymmetry lifts the degeneracy of the $1S_{3/2}$ ground hole states. The asymmetry has three sources: the intrinsic asymmetry of the hexagonal lattice structure of the crystal's field,[34] the nonspherical shape of the finite NC,[35] and an axial asymmetry of confined potential V_h in alloyed nonspherical NCs.[19] All of them split the fourfold degenerate hole state into two twofold degenerates states with $|j_z|=3/2$ and $|j_z|=1/2$, respectively,

$$E_{1S_{3/2},j_z} = E_{1S_{3/2}} - \frac{\Delta}{2}(j_z^2 - 5/4), \quad (12)$$

where $\Delta=\Delta_{\mathrm{int}}+\Delta_{\mathrm{sh}}+\Delta_{\mathrm{pot}}$. For any CP, calculations similar to the ones conducted in Ref. 35 give the splitting connected with the crystal field in hexagonal NCs

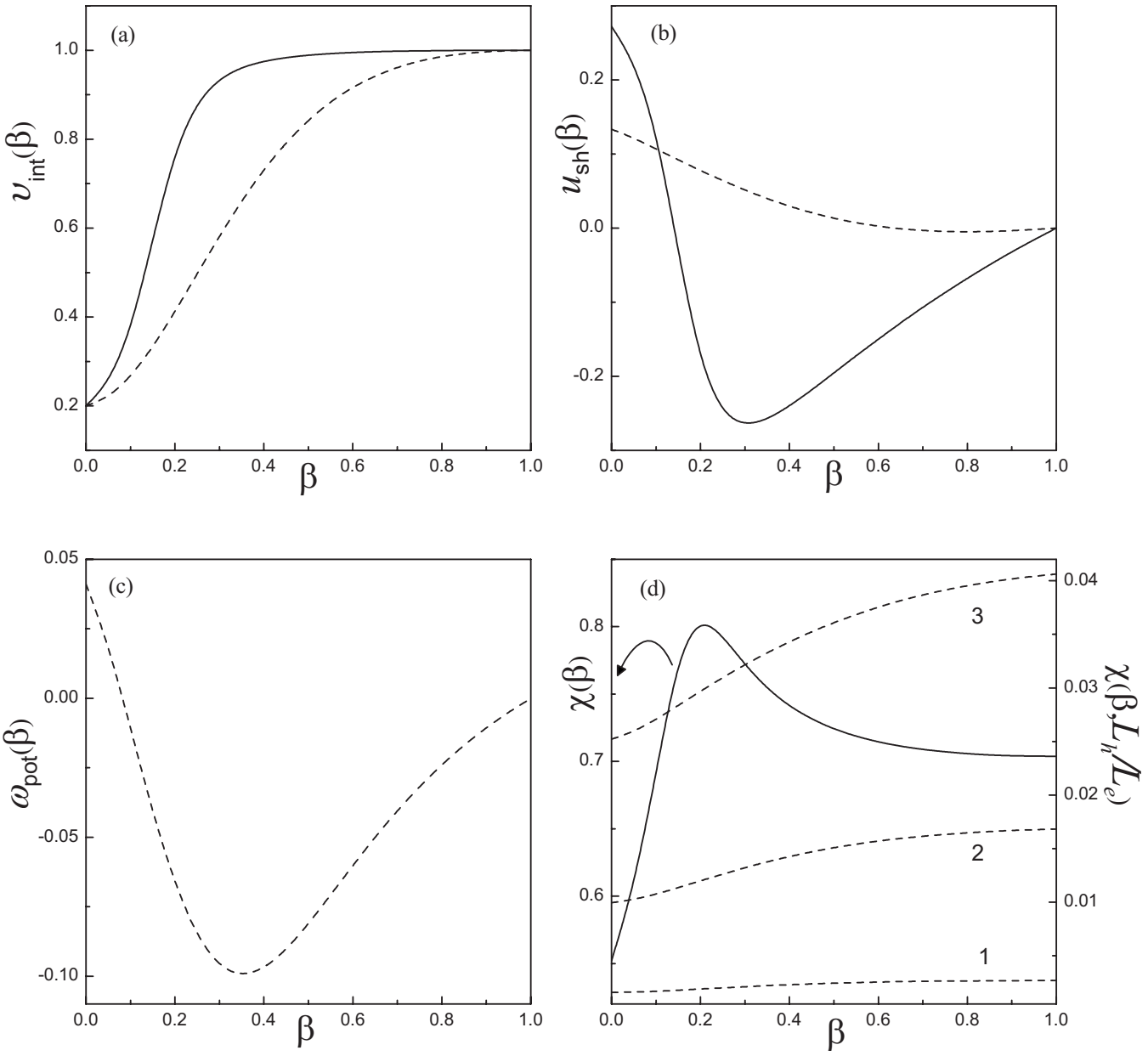

FIG. 2. (a) The dimensionless function $v_{int}(\beta)$ associated with hole level splitting due to the hexagonal lattice structure for the standard and parabolic CPs described in the text as the functions of the light-hole to heavy-hole effective mass ratio β shown by solid and dashed lines, respectively. (b) The dimensionless function $u_{sp}(\beta)$ associated with hole level splitting due to the effect of the NC ellipsoidal shape on the hole kinetic energy for standard and parabolic CPs shown by solid and dashed lines, respectively. (c) The dimensionless function $\omega_{pot}(\beta)$ associated with hole level splitting due to the effect of the NC ellipsoidal shape on the potential energy of the hole confined in spherical parabolic CP. (d) The dimensionless function $\chi(\beta)$ describing the exciton level splitting due to the electron-hole exchange interaction is shown for standard and parabolic CPs for electrons and holes by the solid and dashed lines, respectively. The latter ones were calculated for the following ratios (1) $L_h/L_e=0.25$, (2) $L_h/L_e=0.5$, and (3) $L_h/L_e=0.75$.

$$\Delta_{int} = \Delta_{cr} v_{int} = \Delta_{cr} \int dr r^2 [R_0^2(r) - (3/5) R_2^2(r)], \quad (13)$$

where Δ_{cr} is the splitting between the $|M|=3/2$ and $|M|=1/2$ valence band states in the bulk hexagonal semiconductor caused by the crystal field. In the case of standard boundary conditions and parabolic CP v_{int} depends only on the ratio β and the $|j_z|=3/2$ state is always the ground hole state.[34] In any CP v_{int} increases from 0.2 for $\beta=0$ to 1 for $\beta=1$. The value of v_{int} at $\beta=0$ is determined by Eq. (8) resulting in $\int R_2^2 r^2 dr = \int R_0^2 r^2 dr = 1/2$. For $\beta=1$, $v_{int}=1$ is explained by the vanishing of R_2. The complete dependence of $v_{int}(\beta)$ for both CPs is shown in Fig. 2(a).

The splitting of the ground $j=3/2$ hole state in nonspherical (ellipsoidal) NCs is connected with the difference in a kinetic energy of the holes with $|j_z|=3/2$ and $|j_z|=1/2$.[35] The related splitting can be written in the following form:[35,36]

$$\Delta_{\rm sh} = 2\mu u_{\rm sh} E_{1s_{3/2}}(\beta) = \frac{\mu\hbar^2}{3m_h}\left[I_1 - \frac{1}{5}I_2 + \frac{4}{5}I_3 - \frac{1}{\beta}\left(I_1 - \frac{1}{5}I_2 - \frac{4}{5}I_3\right)\right], \quad (14)$$

where the ellipticity of NCs, $\mu = c/b - 1$, is characterized by the ratio c/b of its major to minor axes, and is positive (negative) in prolate (oblate) NCs, and

$$I_1 = \int r^2 dr \left[\frac{dR_0(r)}{dr}\right]^2,$$

$$I_2 = \int r^2 dr \left\{\left[\frac{dR_2(r)}{dr}\right]^2 + \frac{6R_2(r)^2}{r^2}\right\},$$

$$I_3 = \int r^2 dr R_2(r)\left[\frac{d^2R_0(r)}{dr^2} - \frac{dR_0(r)}{rdr}\right]. \quad (15)$$

For both CPs, $u_{\rm sh}$ depends only on the ratio β. In the case of standard boundary conditions, $u_{\rm sh}$ changes from the value 4/15 at $\beta=0$ to zero at $\beta=1$ and changes its sign from positive to negative with the increase of β at $\beta \approx 0.14$.[35] In the case of the considered parabolic potential, $u_{\rm sh}$ changes from the value 2/15 at $\beta=0$ to zero at $\beta=1$ and changes its sign from positive to negative with the increase in β at $\beta \approx 0.63$. The value of $u_{\rm sh}$ at $\beta=0$ is determined by Eq. (8) which gives $I_1=I_2=I_3$ and $I_1=E_{1S_{3/2}}(0)m_h/\hbar^2$ $[1/2E_{1S_{3/2}}(0)m_h/\hbar^2]$ for the standard boundary conditions (parabolic potential). The differences in $u_{\rm sh}$ are connected with the contribution of the potential energy to $E_{1S_{3/2}}(0)$ in the case of parabolic CP. The splitting vanishes at $\beta=1$ due to vanishing of R_2. The dependence of $u_{\rm sh}(\beta)$ for both CPs is shown in Fig. 2(b).

The asymmetry of the NC shape should also lead to a small asymmetry of the hole confinement potential, $V_h(\boldsymbol{r})$, in SCNCs. In this case the asymmetric potential could be written in the following forms:

$$V_h(\boldsymbol{r}) = \frac{m_h\omega_h^2}{2}\left[r^2 + 2\mu\left(z^2 - \frac{1}{3}r^2\right)\right]. \quad (16)$$

A straightforward calculation gives us the following additional splitting:

$$\Delta_{\rm pot} = 2\mu \cdot \hbar\omega_h \cdot \omega_{\rm pot}(\beta) = -\frac{4\mu}{15}\hbar\omega_h \cdot (L_h)^{-2}\int drr^4 R_0(r)R_2(r). \quad (17)$$

The function $\omega_{\rm pot}(\beta)$ shown in Fig. 2(c) decreases from value 0.04 at $\beta=0$, changes sign at $\beta \approx 0.1$, and goes to zero at $\beta=1$. Thus, the total asymmetry splitting, $\Delta(\beta,a)$, depends generally on the light-hole to heavy-hole effective mass ratio β, on the NC radius a and on the type of the spatial confinement potential.

B. Exciton states

To consider optical transitions between exciton and biexciton states, we must describe the fine structure of excitons in NCs. The fine structure of single-exciton spectra was studied in Refs. 26 and 25. The theory completely describes the PL of CdSe NCs as well as the resonant PL excitation spectra.[27] For alloyed NCs where holes are localized at the NC center we must, however, generalize the theory developed in Ref. 25.

The ground exciton state in spherical NCs of zinc-blende semiconductors is characterized by the total exciton momentum $\boldsymbol{F}$, which has two values: 2 (ground state) and 1 (excited state). In cubic semiconductor NCs with nonspherical shape and NCs with wurzite lattice structure, these states are split into five excitons, each of which is characterized by the projection of the total momentum on the hexagonal axis F.[25] The fine structure of the exciton is strongly affected by e-h exchange interaction enhanced in NCs, which could generally be written in terms of electron and hole radial functions. The strength of this interaction connected with the short-range exchange interaction is described by the energy parameter η (Ref. 25)

$$\eta = \frac{a_0^3}{6\pi}\varepsilon_{\rm exch}\int_0^a drr^2 R_e^2(r)[R_0^2(r) + 0.2R_2^2(r)], \quad (18)$$

where a_0 is the lattice constant and $\varepsilon_{\rm exch}$ is the exchange constant. In CdSe this constant was extracted from the bulk exciton splitting: $\varepsilon_{\rm exch}=450$ meV.[25] In the case of impenetrable CP, the energy parameter can be rewritten as[25] $\eta=(2/\pi)\varepsilon_{\rm exch}(a_0/a)^3\chi(\beta)$ in terms of the dimensionless function $\chi(\beta)$

$$\chi(\beta) = (1/12)a^3\int_0^a drr^2 R_e^2(r)[R_0^2(r) + 0.2R_2^2(r)] \quad (19)$$

that depends only on the ratio of light to heavy-hole effective masses, β. In the case of the parabolic CP, one can write $\eta=(2/\pi)\varepsilon_{\rm exch}(a_0/L_h)^3\chi(\beta,L_h/L_e)$ in terms of the dimensionless function $\chi(\beta,L_h/L_e)$

$$\chi(\beta,L_h/L_e) = (1/12)L_h^3\int_0^\infty drr^2 R_e^2(r)[R_0^2(r) + 0.2R_2^2(r)]. \quad (20)$$

The dependence of the functions χ on β for the standard boundary conditions and for the parabolic confinement with $L_h/L_e=0.25$, $L_h/L_e=0.5$, and $L_h/L_e=0.75$ is shown in Fig. 2(d).

Thus, the short-range electron-hole exchange interaction described by $\eta(\beta,a)$, depends generally on the light-hole to heavy-hole effective mass ratio β, on the NC radius a and on the type of the CP. With these generalizations for η and Δ one can describe the fine structure of the band-edge exciton in a NC of any semiconductor with degenerate valence band with any type of spatial confinement, using the expressions from Ref. 25. There are five-band-edge exciton states. The optically forbidden Dark exciton has total angular momentum projection $F=\pm 2$. Its energy is

$$\epsilon_2 = -3\eta/2 - \Delta/2. \quad (21)$$

There are two, twofold degenerate states with total angular momentum projection $F=\pm 1$. Their energy is

$$\epsilon_1^{\mathrm{U,L}} = \eta/2 \pm \sqrt{\frac{(2\eta-\Delta)^2}{4} + 3\eta^2} \tag{22}$$

for the upper (U) and lower (L) states, where U and L correspond to "+" and "−" signs in the equation, respectively. Finally there are two states with total angular momentum projection $F=0$. Their energies are described as

$$\epsilon_0^{\mathrm{U,L}} = \eta/2 + \Delta/2 \pm 2\eta \tag{23}$$

for the U and L states, where U and L correspond to + and − signs in the equation, respectively.

The wave functions, $\Psi_F(\boldsymbol{r}_\mathrm{e},\boldsymbol{r}_\mathrm{h})$, of all five exciton states were expressed in Ref. 25 via a linear combination of the direct products of independent electron and hole wave functions $\Psi_{\alpha,M}(\boldsymbol{r}_\mathrm{e},\boldsymbol{r}_\mathrm{h})=\Psi_\alpha^\mathrm{e}(\boldsymbol{r}_\mathrm{e})\Psi_M^\mathrm{h}(\boldsymbol{r}_\mathrm{h})$ with $F=\alpha+M$. Equations (17)–(23) describing these wave functions in Ref. 25, however, contain misprints and we write the corrected expressions here. For the exciton state with $|F|=2$, the respective wave functions are[25]

$$\Psi_{-2}(\boldsymbol{r}_\mathrm{e},\boldsymbol{r}_\mathrm{h}) = \Psi_{\downarrow,-3/2}(\boldsymbol{r}_\mathrm{e},\boldsymbol{r}_\mathrm{h}), \quad \Psi_2(\boldsymbol{r}_\mathrm{e},\boldsymbol{r}_\mathrm{h}) = \Psi_{\uparrow,3/2}(\boldsymbol{r}_\mathrm{e},\boldsymbol{r}_\mathrm{h}). \tag{24}$$

For the two levels with $|F|=1$, the corresponding wave functions for the states with $F=+1$ are

$$\Psi_1^\mathrm{U}(\boldsymbol{r}_\mathrm{e},\boldsymbol{r}_\mathrm{h}) = -iC^+\Psi_{\uparrow,1/2}(\boldsymbol{r}_\mathrm{e},\boldsymbol{r}_\mathrm{h}) + C^-\Psi_{\downarrow,3/2}(\boldsymbol{r}_\mathrm{e},\boldsymbol{r}_\mathrm{h}),$$

$$\Psi_1^\mathrm{L}(\boldsymbol{r}_\mathrm{e},\boldsymbol{r}_\mathrm{h}) = +iC^-\Psi_{\uparrow,1/2}(\boldsymbol{r}_\mathrm{e},\boldsymbol{r}_\mathrm{h}) + C^+\Psi_{\downarrow,3/2}(\boldsymbol{r}_\mathrm{e},\boldsymbol{r}_\mathrm{h}) \tag{25}$$

while for the states with $F=-1$, the wave functions are

$$\Psi_{-1}^\mathrm{U}(\boldsymbol{r}_\mathrm{e},\boldsymbol{r}_\mathrm{h}) = -iC^-\Psi_{\uparrow,-3/2}(\boldsymbol{r}_\mathrm{e},\boldsymbol{r}_\mathrm{h}) + C^+\Psi_{\downarrow,-1/2}(\boldsymbol{r}_\mathrm{e},\boldsymbol{r}_\mathrm{h}),$$

$$\Psi_{-1}^\mathrm{L}(\boldsymbol{r}_\mathrm{e},\boldsymbol{r}_\mathrm{h}) = +iC^+\Psi_{\uparrow,-3/2}(\boldsymbol{r}_\mathrm{e},\boldsymbol{r}_\mathrm{h}) + C^-\Psi_{\downarrow,-1/2}(\boldsymbol{r}_\mathrm{e},\boldsymbol{r}_\mathrm{h}), \tag{26}$$

where

$$C^\pm = \sqrt{\frac{D\pm f}{2D}}, \tag{27}$$

$f=\Delta/2-\eta$ and $D=\sqrt{f^2+3\eta^2}$. For the two $F=0$ exciton levels, the corresponding wave functions are described by[25]

$$\Psi_0^{\mathrm{U,L}}(\boldsymbol{r}_\mathrm{e},\boldsymbol{r}_\mathrm{h}) = \frac{1}{\sqrt{2}}(\mp i\Psi_{\uparrow,-1/2}(\boldsymbol{r}_\mathrm{e},\boldsymbol{r}_\mathrm{h}) + \Psi_{\downarrow,1/2}(\boldsymbol{r}_\mathrm{e},\boldsymbol{r}_\mathrm{h})), \tag{28}$$

where superscripts U and L correspond to the upper (−) and the lower (+) signs, respectively.

C. Ground biexciton state

The Pauli principle limits the number of biexciton states that could be formed at the band edge of NCs of direct band-gap semiconductors because it allows only two electrons with opposite spin directions to occupy the ground $1S_e$ electron level. The singlet configuration of electron spins in the ground biexciton state is described by the following wave function:

$$\Phi_0^{2\mathrm{e}}(\boldsymbol{r}_{\mathrm{e}1},\boldsymbol{r}_{\mathrm{e}2}) = \frac{1}{\sqrt{2}}[\Psi_{1/2}^\mathrm{e}(\boldsymbol{r}_{\mathrm{e}1})\Psi_{-1/2}^\mathrm{e}(\boldsymbol{r}_{\mathrm{e}2}) - \Psi_{-1/2}^\mathrm{e}(\boldsymbol{r}_{\mathrm{e}1})\Psi_{1/2}^\mathrm{e}(\boldsymbol{r}_{\mathrm{e}2})], \tag{29}$$

where $\Psi_{\pm1/2}^\mathrm{e}(\boldsymbol{r}_\mathrm{e})$ are the single-electron wave functions described in Eq. (1). Importantly the e-h exchange interaction, which plays such an important role in the energy spectra of the band-edge exciton, vanishes completely in the biexciton due to the exact cancellation of the two electron contributions, which have opposite signs.

Implication of the Pauli exclusion principle to the two holes of the biexciton occupying the $1S_{3/2}$ level is nontrivial. Generally, the two holes with momentum $|\boldsymbol{j}_1|=|\boldsymbol{j}_2|=3/2$ according to the momentum summation rule $\boldsymbol{J}=\boldsymbol{j}_1+\boldsymbol{j}_2$ could form four states with the total angular momentum $J=3$, 2, 1, and 0. The wave functions of these states can generally be written

$$\Phi_{J,J_z}^{2\mathrm{h}}(\boldsymbol{r}_1,\boldsymbol{r}_2) = (-1)^{J_z}\sqrt{2J+1}\sum_{M_1+M_2=J_z} \times \begin{pmatrix} 3/2 & 3/2 & J \\ M_1 & M_2 & -J_z \end{pmatrix} \Psi_{M_1}^\mathrm{h}(\boldsymbol{r}_1)\Psi_{M_2}^\mathrm{h}(\boldsymbol{r}_2), \tag{30}$$

where J_z is the projection of the total momentum $\boldsymbol{J}$ on z axis. The Pauli hole permutation requirement applied to the wave function described by Eq. (30), however, allows only the two nontrivial solutions. As a result, the two holes occupying the $1S_{3/2}$ level can only be in a fivefold degenerate state with total momentum $J=2$ and a state with $J=0$.[18]

Hole-hole exchange interaction splits the ground biexciton into the two states with total momentum $J=2$ and $J=0$. The straightforward calculation of the h-h Coulomb interaction with the functions from Eq. (30) gives the energy of the corresponding levels

$$E_J(\beta) = E_{bi}(\beta) - \frac{\Delta_\mathrm{exch}(\beta)}{8}(4J-5), \tag{31}$$

where $E_{bi}(\beta)$ is the band-edge biexciton energy and exchange splitting $\Delta_\mathrm{exch}(\beta)=E_0(\beta)-E_2(\beta)$ can be written in the following form:[18]

$$\Delta_\mathrm{exch}(\beta) = \frac{e^2}{2\kappa}\frac{64}{25}\int\int r_1^2 r_2^2 dr_1 dr_2 \frac{r_<^2}{r_>^3} R_0(r_1)R_2(r_1)R_0(r_2)R_2(r_2), \tag{32}$$

where κ is the dielectric constant of the semiconductor and $r_<=min\{r_1,r_2\}$, $r_>=max\{r_1,r_2\}$. One can see that in the spherical NCs, the ground biexciton state has total momentum $J=2$. The splitting is inversely proportional to the characteristic confinement length for holes, a^*, and depends on the ratio of light to heavy-hole effective masses. It generally can be written as

$$\Delta_\mathrm{exch}(\beta) = \frac{e^2}{2\kappa a^*}\gamma(\beta), \tag{33}$$

where $a^*=a$ in the case of NCs with standard CP and $a^*=L_\mathrm{h}$ in the case of the parabolic CP. The corresponding $\gamma(\beta)$

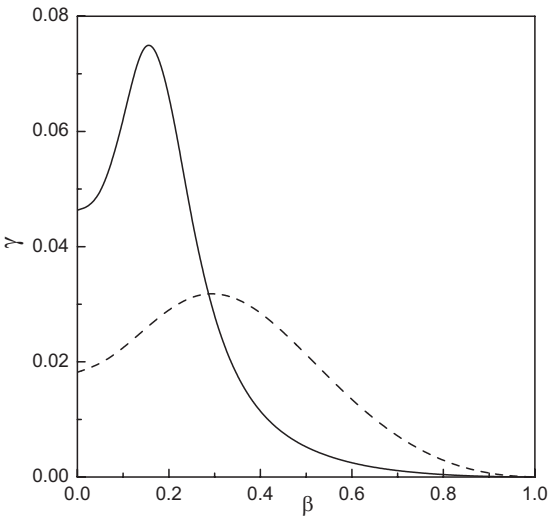

FIG. 3. The dimensionless function $\gamma(\beta)$ describing the biexciton level splitting due to h-h exchange interaction as a function of the ratio of the light to heavy-hole effective masses, β, for the standard and parabolic CPs shown by the solid and dashed lines, correspondingly.

for the two cases are shown in Fig. 3. One can see that $\gamma(\beta)$ is always positive.

The NC asymmetry, which lifts degeneracy of the $1S_{3/2}$ hole state in Eq. (12), results in further splitting of the biexciton states. The corresponding perturbation can be written as

$$\hat{H}_{\rm as}^{\rm 2h} = \hat{H}_{\rm as}^{\rm 1h}(\boldsymbol{r}_1) + \hat{H}_{\rm as}^{\rm 1h}(\boldsymbol{r}_2) = -\frac{\Delta}{2}(\hat{j}_{1z}^2 - 5/4) - \frac{\Delta}{2}(\hat{j}_{2z}^2 - 5/4), \tag{34}$$

where $\hat{j}_{1z}$ and $\hat{j}_{2z}$ are the operators of hole momentum projection acting on the first and second holes, respectively. One can see that the perturbation described by Eq. (34) conserves the total spin projection J_z of the two holes. This perturbations also does not lead to the first-order corrections to the two hole states with $J=2$ and $J=0$: $\langle \Phi_{J,J_z}^{\rm 2h} | \hat{H}_{\rm as}^{\rm 2h} | \Phi_{J,J_z}^{\rm 2h} \rangle = 0$. Indeed, the matrix elements of these perturbations taken between the wave functions of the two hole states can be written

$$\begin{aligned}\langle \Phi_{J_1,J_z}^{\rm 2h} | \hat{H}_{\rm as}^{\rm 2h} | \Phi_{J_2,J_z}^{\rm 2h} \rangle &= 2\sqrt{(2J_1+1)(2J_2+1)} \\ &\times \sum_{M_1+M_2=J_z} \begin{pmatrix} 3/2 & 3/2 & J_1 \\ M_1 & M_2 & -J_z \end{pmatrix} \begin{pmatrix} 3/2 & 3/2 & J_2 \\ M_1 & M_2 & -J_z \end{pmatrix} \\ &\times \langle \Psi_{M_1}^{\rm h}(\boldsymbol{r}) | \hat{H}_{\rm as}^{\rm 1h} | \Psi_{M_1}^{\rm h}(\mathbf{r}) \rangle. \end{aligned} \tag{35}$$

One can see that for $J_1=J_2=J$, the sum in Eq. (35) is zero because $\langle \Psi_{\pm 3/2}^{\rm h}(\boldsymbol{r}) | \hat{H}_{\rm as}^{\rm 1h} | \Psi_{\pm 3/2}^{\rm h}(\boldsymbol{r}) \rangle = -\langle \Psi_{\pm 1/2}^{\rm h}(\boldsymbol{r}) | \hat{H}_{\rm as}^{\rm 1h} | \Psi_{\pm 1/2}^{\rm h}(\boldsymbol{r}) \rangle$. The only nonzero matrix element in Eq. (35) is between states with $J=2$ and $J=0$: $\langle \Phi_{0,0}^{\rm 2h} | \hat{H}_{\rm as}^{\rm 2h} | \Phi_{2,0}^{\rm 2h} \rangle = -\Delta$. As a result, the perturbation matrix taken on the basis of the functions of two independent holes $\Phi_{J,J_z}^{\rm 2h}$ that describes the fine structure of the ground biexciton states can be written

$$\left(\begin{array}{c|cccccc} & |0,0\rangle & |2,0\rangle & |2,2\rangle & |2,1\rangle & |2,-1\rangle & |2,-2\rangle \\ \hline |0,0\rangle & E_0 & -\Delta & 0 & 0 & 0 & 0 \\ |2,0\rangle & -\Delta & E_2 & 0 & 0 & 0 & 0 \\ |2,2\rangle & 0 & 0 & E_2 & 0 & 0 & 0 \\ |2,1\rangle & 0 & 0 & 0 & E_2 & 0 & 0 \\ |2,-1\rangle & 0 & 0 & 0 & 0 & E_2 & 0 \\ |2,-2\rangle & 0 & 0 & 0 & 0 & 0 & E_2 \end{array}\right). \tag{36}$$

The diagonalization of this matrix gives us the energy of the three biexciton levels.

The ground biexciton state has the angular momentum projection $J_z=0$ and the energy

$$E_0^- = E_2(\beta,a) + \frac{\Delta_{\rm exch}(\beta,a)}{2} - \sqrt{\left[\frac{\Delta_{\rm exch}(\beta,a)}{2}\right]^2 + \Delta(\beta,a)^2}, \tag{37}$$

The first excited state has $J_z = \pm 1$, and ± 2 and energy E_2, which is not affected by perturbations connected with NC

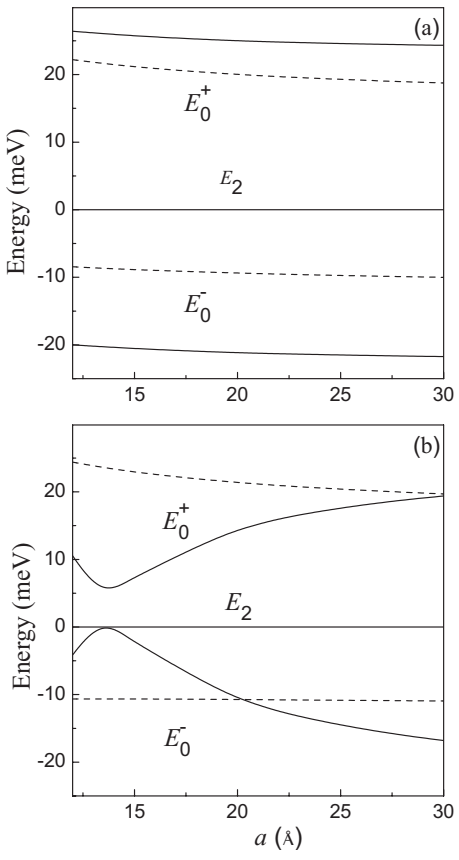

FIG. 4. Size dependence of the biexciton fine structure calculated in (a) spherical and (b) slightly elongated ($\mu=0.1$) CdSe NCs for the standard and parabolic CPs for holes shown by the solid and dashed lines, correspondingly. For the parabolic CP we used the hole wave function with $L_{\rm h}=\sqrt{a\hbar^2/(2m_{\rm h}V_{\rm h}^{off})}$ where $m_{\rm h}=m_0$ and $V_{\rm h}^{off}=0.6$ eV.

asymmetry. Finally the upper biexciton state has $J_z=0$ and the energy:

$$E_0^+ = E_0(\beta,a) - \frac{\Delta_{\rm exch}(\beta,a)}{2} + \sqrt{\left[\frac{\Delta_{\rm exch}(\beta,a)}{2}\right]^2 + \Delta(\beta,a)^2}, \tag{38}$$

For the case when $\Delta_{\rm exch}=0$, the splittings between all biexciton states with $J_z=0$ (the upper and lower levels) and $J_z=\pm 1, \pm 2$ (the middle level) are equal to Δ. The fine structure of the biexciton levels in NCs with different types of confinement is shown in Fig. 4.

The figure shows size dependence of the biexciton fine structure calculated in spherical and slightly elongated ($\mu=0.1$) CdSe NCs. The crystal-field splitting of the hole levels has been taken into account. One can see that the biexciton fine structure in spherical CdSe NCs is almost independent of the NC radius. In the elongated CdSe NCs with standard CP the fine-structure splitting shows the nonmonotonic size dependence. The splitting decreases initially with size, passes through the minimum, and finally increases. This size dependence is controlled by the size dependence of the total splitting of the hole levels. The minimum of the dependence is the most interesting point on this curve. The minimum splitting is reached at the NC size, where the NC shape asymmetry and crystal field exactly compensate their contribution to the splitting of the holes. The corresponding NC has the electronic properties of a spherical NC although it does not have spherical shape. As a result, the NC has just two biexciton states: a fivefold degenerate biexciton with total angular momentum 2 and the state with total angular momentum 0 that should exist only in a spherical cubic NC.[18] In the case of the parabolic CP, this variation in the biexciton fine structure does not take place. First, the contribution of the shape asymmetry to the kinetic energy of holes has another sign in elongated parabolically confined CdSe NCs and this contribution does not compensate for the crystal-field effect. Second, the contributions of the shape asymmetry to the kinetic and potential energy of holes confined in parabolic CdSe NCs have opposite signs and they nearly compensate each other. Thus, one can observe quantitatively different size dependence of the biexciton fine structure in NCs with standard and parabolic confinement.

The wave functions of these band-edge biexciton states can be written as the product

$$\Phi_{J_z}(\boldsymbol{r}_{\rm e1},\boldsymbol{r}_{\rm e2},\boldsymbol{r}_{\rm h1},\boldsymbol{r}_{\rm h2}) = \Phi_0^{\rm 2e}(\boldsymbol{r}_{\rm e1},\boldsymbol{r}_{\rm e2})\Phi_{J_z}^{\rm 2h}(\boldsymbol{r}_{\rm h1},\boldsymbol{r}_{\rm h2}) \tag{39}$$

of the two electron wave function, $\Phi_0^{\rm 2e}(\boldsymbol{r}_{\rm e1},\boldsymbol{r}_{\rm e2})$, defined in Eq. (29) and the two-hole wave functions $\Phi_{J_z}^{\rm 2h}(\boldsymbol{r}_{\rm h1},\boldsymbol{r}_{\rm h2})$. For the biexciton states with the projections $J_z=\pm 1, \pm 2$ these wave functions are the unperturbed wave functions of the biexciton states in spherical potential with the same projection momentum

$$\begin{aligned}\Phi_{\pm 1}^{\rm 2h}(\boldsymbol{r}_{\rm h1},\boldsymbol{r}_{\rm h2}) &= \Phi_{2,\pm 1}^{\rm 2h}(\boldsymbol{r}_{\rm h1},\boldsymbol{r}_{\rm h2}),\\ \Phi_{\pm 2}^{\rm 2h}(\boldsymbol{r}_{\rm h1},\boldsymbol{r}_{\rm h2}) &= \Phi_{2,\pm 2}^{\rm 2h}(\boldsymbol{r}_{\rm h1},\boldsymbol{r}_{\rm h2})\end{aligned} \tag{40}$$

For the biexciton states with $J_z=0$, the corresponding wave functions are linear combinations of those for the states with total momentum 2 and 0

$$\Phi_0^{\rm 2h,\pm}(\boldsymbol{r}_{\rm h1},\boldsymbol{r}_{\rm h2}) = B_2^{\pm}\Phi_{2,0}^{\rm 2h}(\boldsymbol{r}_{\rm h1},\boldsymbol{r}_{\rm h2}) + B_0^{\pm}\Phi_{0,0}^{\rm 2h}(\boldsymbol{r}_{\rm h1},\boldsymbol{r}_{\rm h2}), \tag{41}$$

where

$$B_0^{\pm} = \mp \frac{2\Delta}{\sqrt{4\Delta^2 + D_{\pm}^2}}, \quad B_2^{\pm} = \sqrt{1-(B_0^{\pm})^2} \tag{42}$$

with $D_{\pm}=\Delta_{\rm exch} \mp \sqrt{\Delta_{\rm exch}^2+4\Delta^2}$. Using explicit expressions for the functions $\Phi_{J,J_z}^{\rm 2h}$ we can rewrite Eqs. (40) and (41) in the more useful form

$$\begin{aligned}\Phi_0^{\rm 2h,\pm}(\boldsymbol{r}_{\rm h1},\boldsymbol{r}_{\rm h2}) &= \frac{1}{2}\{(B_2^{\pm}+B_0^{\pm})[\Psi_{3/2}^{\rm h}(\boldsymbol{r}_{\rm h1})\Psi_{-3/2}^{\rm h}(\boldsymbol{r}_{\rm h2}) - \Psi_{-3/2}^{\rm h}(\boldsymbol{r}_{\rm h1})\Psi_{3/2}^{\rm h}(\boldsymbol{r}_{\rm h2})]\\ &\quad + (B_2^{\pm}-B_0^{\pm})[\Psi_{1/2}^{\rm h}(\boldsymbol{r}_{\rm h1})\Psi_{-1/2}^{\rm h}(\boldsymbol{r}_{\rm h2}) - \Psi_{-1/2}^{\rm h}(\boldsymbol{r}_{\rm h1})\Psi_{1/2}^{\rm h}(\boldsymbol{r}_{\rm h2})]\},\\ \Phi_{\pm 1}^{\rm 2h}(\boldsymbol{r}_{\rm h1},\boldsymbol{r}_{\rm h2}) &= \pm\frac{1}{\sqrt{2}}[\Psi_{\pm 3/2}^{\rm h}(\boldsymbol{r}_{\rm h1})\Psi_{\mp 1/2}^{\rm h}(\boldsymbol{r}_{\rm h2}) - \Psi_{\mp 1/2}^{\rm h}(\boldsymbol{r}_{\rm h1})\Psi_{\pm 3/2}^{\rm h}(\boldsymbol{r}_{\rm h2})],\\ \Phi_{\pm 2}^{\rm 2h}(\boldsymbol{r}_{\rm h1},\boldsymbol{r}_{\rm h2}) &= \pm\frac{1}{\sqrt{2}}[\Psi_{\pm 3/2}^{\rm h}(\boldsymbol{r}_{\rm h1})\Psi_{\pm 1/2}^{\rm h}(\boldsymbol{r}_{\rm h2}) - \Psi_{\pm 1/2}^{\rm h}(\boldsymbol{r}_{\rm h1})\Psi_{\pm 3/2}^{\rm h}(\boldsymbol{r}_{\rm h2})].\end{aligned} \tag{43}$$

Using Eq. (42) one can show that $B_0^{\pm}=\mp(\Delta/|\Delta|)/\sqrt{2}$ and $B_2^{\pm}=1/\sqrt{2}$ if $\Delta_{\rm exch}\ll|\Delta|$. Only in this case, the wave functions of the equally spaced biexciton triplet is constructed solely from the holes with the same module of the angular momentum projection: $\pm 3/2$ if $\Delta>0$ or solely from the $\pm 1/2$ if $\Delta<0$. Even in this limit, however, the hole states are always a mixture of light and heavy holes and are not the heavy-hole states as mistakenly written in Ref. 17. The op-

posite limiting case, $\Delta_{exch} \gg |\Delta|$, describes the spherical cubic NCs. This case can also be realized in some size range of the elongated NCs, for which $\Delta(a) \approx 0$ as one can see in Fig. 4(b). In this case Eq. (42) gives $B_0^- = 0$ and $B_2^- = 1$ for the lower ground state with energy $E_0^- = E_2$; and $|B_0^+| = 1$ and $B_2^- = 0$ for the upper excited state with energy $E_0^+ = E_0$. One can easily verify using Eq. (42), that $B_0^{-2} + B_0^{+2} = B_2^{-2} + B_2^{+2} = 1$. As a result, the admixture of the $J=0$ wave function to the lowest 0^- state described by $|B_0^-|$ is always the same as the admixture of the $J=2$ wave function to the upper 0^+ state described by $|B_2^+|$. As one can see in Fig. 4(b), the anticrossing of the biexciton energy levels takes place at NC radius where $\Delta(a)=0$ due to the nonzero h-h exchange interaction. Thus the account of the h-h exchange interaction is very important for the proper description of the size-dependent biexciton energy structure.

III. BIEXCITON-EXCITON TRANSITION PROBABILITIES

Both the absorption spectra of NCs with an already created exciton and the biexciton PL are controlled by optical transitions between exciton and biexcitons states. Let us first consider the selection rules for the biexciton-exciton optical transitions. Following Elliott,[37] we can write the probability of the transitions between an exciton state, X (± 2, $\pm 1^{L,U}$, and $\pm 0^{L,U}$) and a biexciton state, BX ($0^{\pm}$, ± 1, and ± 2), as the square of the following matrix element:

$$\begin{aligned} T(X,BX) &= \sum_{\substack{i,j,k,m=1,2 \\ i\neq k, j\neq m}} |\langle \Psi_F^X(\boldsymbol{r}_{ei}, \boldsymbol{r}_{hj}) \\ &\quad \times \delta(\boldsymbol{r}_{ek} - \boldsymbol{r}_{hm}) | \boldsymbol{e}\hat{\boldsymbol{p}} | \Phi_{J_z}^{BX}(\boldsymbol{r}_{e1}, \boldsymbol{r}_{e2}, \boldsymbol{r}_{h1}, \boldsymbol{r}_{h2}) \rangle|^2 \\ &= 4 |\langle \Psi_F^X(\boldsymbol{r}_{e1}, \boldsymbol{r}_{h1}) \delta(\boldsymbol{r}_{e2} - \boldsymbol{r}_{h2}) | \boldsymbol{e}\hat{\boldsymbol{p}} | \\ &\quad \times \Phi_{J_z}^{BX}(\boldsymbol{r}_{e1}, \boldsymbol{r}_{e2}, \boldsymbol{r}_{h1}, \boldsymbol{r}_{h2}) \rangle|^2. \end{aligned} \tag{44}$$

Here $\boldsymbol{e}$ is the polarization of the emitted or absorbed light and the momentum operator $\hat{\boldsymbol{p}}$ acts only on the valence band Bloch functions. The calculation of $T(X,BX)$ with the wave functions of excitons, Ψ_F^X, defined in Eqs. (24)–(26) and (28) and biexcitons, $\Phi_{J_z}^{BX} = \Phi_0^{2e} \Phi_{J_z}^{2h}$, defined in Eqs. (29), (40), and (41) is straightforward but cumbersome because the hexagonal axes of a NC ensemble are randomly oriented relative to the light propagation of emission directions. First, let us consider $T(X,BX)$'s responsible for the two most important nonlinear optical processes in NCs: (i) the radiative decay of the ground biexciton state and (ii) the resonant photoexcitation of the ground exciton state, which is critical in all pump-probe experiments.

The ground biexciton state has zero angular momentum projection. It can radiatively decay in all exciton states except the state with angular momentum projection ± 2. If the NCs were oriented, according to the selection rules, the transitions to the states with the angular momentum projection ± 1 should be accompanied by emission of circularly polarized light along their hexagonal axes while transitions to the state with angular momentum 0 should be accompanied by emission of linear polarized light perpendicular to these axes. For any other NC orientation, the biexciton emission is not polarized and generally can be considered as an emission of linear polarized light with an arbitrary polarization plane.

A. Transition probabilities caused by linear polarized light

For linear polarized light, $\boldsymbol{e}\hat{\boldsymbol{p}}$ in Eq. (44) can be written

$$\boldsymbol{e}\hat{\boldsymbol{p}} = e_z \hat{p}_z + \frac{1}{2}[e_- \hat{p}_+ + e_+ \hat{p}_-], \tag{45}$$

where z is the direction of the hexagonal axis of the NC, $e_{\pm} = e_x \pm i e_y$, $\hat{p}_{\pm} = \hat{p}_x \pm i \hat{p}_y$, and $e_{x,y}$ and $\hat{p}_{x,y}$ are the components of the polarization vector and the momentum operator, respectively, that are perpendicular to the NC hexagonal axis.

Let us calculate the corresponding $T(X, 0^-; \pi)$ connected with linear polarized light. These matrix elements can be used to describe of a radiative decay of the biexciton ground state into different exciton states.[38] The transition probability to the exciton state with $F = \pm 2$ is described by $T(\pm 2, 0^-) = 0$ and is equal to zero. The biexciton decay into the exciton U pper and L over states with $F=0$ is described by

$$\begin{aligned} &T(0^{U,L}, 0^-; \pi) \\ &\quad = 4 |\langle \Psi_0^{U,L}(\boldsymbol{r}_{e1}, \boldsymbol{r}_{h1}) \delta(\boldsymbol{r}_{e2} - \boldsymbol{r}_{h2}) | \boldsymbol{e}\hat{\boldsymbol{p}} | \Phi_0^-(\boldsymbol{r}_{e1}, \boldsymbol{r}_{e2}, \boldsymbol{r}_{h1}, \boldsymbol{r}_{h2}) \rangle|^2 \\ &\quad = (B_2^- - B_0^-)^2 \frac{(1 \pm 1)^2}{6} K P^2 \cos^2 \theta, \end{aligned} \tag{46}$$

where $P = -i\langle S | \hat{p}_z | Z \rangle$ is the Kane transition matrix element, θ is the angle between the vector polarization of light $\boldsymbol{e}$ and the hexagonal axis of the NC, and K is the square of the overlap integral between the electron and hole wave functions[25]

$$K = \left| \int dr r^2 R_e(r) R_0(r) \right|^2. \tag{47}$$

One can see from Eq. (46), that the biexciton transitions to the L over exciton states with $F=0$ are forbidden, while the transitions to the U pper exciton state are allowed, contrary to the selection rules described by Ref. 17. It is easy to show that $T(0^U, 0^-; \pi)$ vanishes only if one neglects the h-h exchange interaction in the biexciton.

The relative probability of biexciton decay into the two U pper and two L over exciton states with $F = \pm 1$ are described by

$$\begin{aligned} 2T(\pm 1^{U,L}, 0^-; \pi) &= 8 |\langle \Psi_{\pm 1}^{U,L}(\boldsymbol{r}_{e1}, \boldsymbol{r}_{h1}) \delta(\boldsymbol{r}_{e2} - \boldsymbol{r}_{h2}) | \boldsymbol{e}\hat{\boldsymbol{p}} | \\ &\quad \times \Phi_0^-(\boldsymbol{r}_{e1}, \boldsymbol{r}_{e2}, \boldsymbol{r}_{h1}, \boldsymbol{r}_{h2}) \rangle|^2. \end{aligned} \tag{48}$$

Here the additional factor 2 is connected with the degeneracy of the exciton state with $F = \pm 1$ and the fact that $T(+1^{U,L}, 0^-; \pi) = T(-1^{U,L}, 0^-; \pi)$. A straightforward calculation results in

$$\tilde{T}(1^{U,L}, 0^-; \pi) = 2T(\pm 1^{U,L}, 0^-; \pi) = \frac{2}{3} K P^2 \sin^2 \theta N_{U,L}^- \tag{49}$$

with

$$N^{-}_{\mathrm{U,L}} = (B^{-}_{0})^2 N^{\mathrm{U,L}}_{1} + (B^{-}_{2})^2 N^{\mathrm{U,L}}_{2} + B^{-}_{0} B^{-}_{2} N^{\mathrm{U,L}}_{02}, \tag{50}$$

$$N^{\mathrm{U,L}}_{1} = \left(\frac{2D \mp f \pm 3\eta}{4D} \right), \quad N^{\mathrm{U,L}}_{2} = \left(\frac{2D \mp f \mp 3\eta}{4D} \right),$$

$$N^{\mathrm{U,L}}_{02} = \left(\frac{D \mp 2f}{2D} \right), \tag{51}$$

where upper signs and lower signs describe the transition probabilities to the U pper and L over levels, respectively. One can see from Eq. (50) that the transitions to both exciton levels are allowed, contrary to the selection rules described in Ref. 17. The transition probability to the U pper exciton state vanishes only if one completely neglects the h-h and e-h exchange interaction.

The relative probability of the ground biexciton radiative decay into the different exciton states can be obtained after integration of Eqs. (46) and (50) over all possible directions of emitted light. These probabilities can be expressed via Eqs. (46) and (50) with $\cos^2\theta$ and $\sin^2\theta$ replaced by 1/3 and 2/3, respectively.

Let us now consider the resonant photoexcitation of the ground exciton state with $F=\pm 2$ to the biexciton states. According to the selection rules discussed above, the photoexcitation could occur only into fourfold degenerate biexciton states with angular momentum projection $J_z=\pm 2$ or $J_z=\pm 1$. The polarization properties of the photoexcitation would be very simple if the NC were aligned along the light propagation direction. In this case, only the $\sigma^{\pm}$ circularly polarized light would create the $J_z=\pm 1$ biexciton state. However the NCs are randomly oriented and both the linear and circularly polarized light create biexcitons with different probabilities.

Let us consider first the effect of *linear polarized light*. If the exciton in a NC occupies the ground exciton state with $F=+2$ the transition probability is proportional to the following sum:

$$\begin{aligned} &T(+2,+2;\pi) + T(+2,+1;\pi) \\ &\quad = 4\left|\langle \Psi_{+2}(\boldsymbol{r}_{\mathrm{e1}},\boldsymbol{r}_{\mathrm{h1}}\delta(\boldsymbol{r}_{\mathrm{e2}}-\boldsymbol{r}_{\mathrm{h2}})|\boldsymbol{e}\hat{\boldsymbol{p}}|\Phi_{+2}(\boldsymbol{r}_{\mathrm{e1}},\boldsymbol{r}_{\mathrm{e2}},\boldsymbol{r}_{\mathrm{h1}},\boldsymbol{r}_{\mathrm{h2}})\rangle\right|^2 \\ &\qquad + 4\left|\langle \Psi_{+2}(\boldsymbol{r}_{\mathrm{e1}},\boldsymbol{r}_{\mathrm{h1}})\,\delta(\boldsymbol{r}_{\mathrm{e2}}-\boldsymbol{r}_{\mathrm{h2}})|\boldsymbol{e}\hat{\boldsymbol{p}}|\Phi_{+1}(\boldsymbol{r}_{\mathrm{e1}},\boldsymbol{r}_{\mathrm{e2}},\boldsymbol{r}_{\mathrm{h1}},\boldsymbol{r}_{\mathrm{h2}})\rangle\right|^2 \\ &\quad = \frac{KP^2}{6}[3\cos^2\theta + 1]. \end{aligned} \tag{52}$$

The identical expression with + replaced by − describes the photoexcitation of the ground $F=-2$ exciton leading to $T(-2,-2;\pi)+T(-2,-1;\pi)=T(+2,+2;\pi)+T(+2,+1;\pi)$ so that the total excitation probability from the exciton ground state is given by $\tilde{T}(2,2;\pi)=2[T(+2,+2;\pi)+T(+2,+1;\pi)]$.

B. Transition probabilities caused by circularly polarized light

Let us consider now the photoexcitation of the ground exciton state by circularly polarized light. The selection rules and the relative transition probabilities in this case are determined by the matrix element of the operator $1/\sqrt{2}e_{\pm}\hat{p}_{\mp}$, where the polarization vector, $e_{\pm}=e_x \pm ie_y$, and the momentum, $\hat{p}_{\pm}=\hat{p}_x \pm i\hat{p}_y$, lie in the plane that is perpendicular to the light-propagation direction. In vector representation, this operator can be written as in Ref. 39

$$\frac{1}{\sqrt{2}}e_{\pm}\hat{p}_{\mp} = \frac{1}{\sqrt{2}}(\boldsymbol{e}\hat{\boldsymbol{p}} \pm i\boldsymbol{e}'\hat{\boldsymbol{p}}), \tag{53}$$

where $\boldsymbol{e}\perp\boldsymbol{c}$, $\boldsymbol{c}$ is the unit vector parallel to the light propagation direction and $\boldsymbol{e}'=(\boldsymbol{e}\times\boldsymbol{c})$; as a result of the $\boldsymbol{e}'$ definition, the scalar product $(\boldsymbol{e}\boldsymbol{e}')=0$. To calculate the matrix element in Eq. (44), we expand the operator of Eq. (53) in coordinates that are connected with the direction of the hexagonal axis of the NCs (z direction)

$$\frac{1}{\sqrt{2}}e_{\pm}\hat{p}_{\mp} = \frac{1}{\sqrt{2}}\boldsymbol{\epsilon}^{\pm}\hat{\boldsymbol{p}} = \frac{1}{\sqrt{2}}\left(\epsilon^{\pm}_{z}\hat{p}_{z} + \frac{1}{2}[\epsilon^{\pm}_{+}\hat{p}_{-} + \epsilon^{\pm}_{-}\hat{p}_{+}]\right), \tag{54}$$

where $\boldsymbol{\epsilon}^{\pm}=\boldsymbol{e}\pm i\boldsymbol{e}'$ and $\epsilon^{\pm}_{\pm}=\epsilon^{\pm}_{x}\pm i\epsilon^{\pm}_{y}$. Substituting Eq. (54) into Eq. (44) we obtain the relative values of the optical transition probability between exciton and biexciton states coursed by the absorption/emission of the $\sigma^{\pm}$ polarized light.

In the NCs oriented under angle θ_k to the light-propagation direction, the probability of the transitions between the $F=2$ exciton and $J_z=1$ biexciton states and the $F=-2$ exciton and $J_z=-1$ biexciton states initiated by the $\sigma^{\pm}$ polarized light, are given, respectively, by

$$T(+2,+1;\sigma^{\mp}) = T(-2,-1;\sigma^{\pm}) = \frac{KP^2}{12}(1 \pm \cos\theta_k)^2. \tag{55}$$

The probabilities of the transition between the $F=+2$ ($F=-2$) exciton and $J_z=+2$ ($J_z=-2$) biexciton states initiated by the $\sigma^{\pm}$ polarized light are given by

$$T(\pm 2,\pm 2;\sigma^{\pm}) = \frac{KP^2}{3}\sin^2\theta_k. \tag{56}$$

At high temperature or during transient relaxation time, one can observe PL from the upper biexciton states or the photoexcitation of the NC where an exciton occupies a higher band-edge state. For example, the intermediate biexciton state with energy E_2 can decay radiatively to all possible exciton states with different polarizations of emitted light. The unrelaxed excitons also strongly affect the selection rules and intensity of the NC resonant photoexcitation. In Tables I and II we summarize the relative transition probabilities described by Eq. (44) for linear and circularly polarized light, respectively.

The relative transition probabilities are given in the $KP^2/6$ units. In the case of the standard CP the value of K is independent of crystal size and depends only on β.[25] In the case of the parabolic CP the value of K depends additionally on the ratio of the hole and electron oscillator lengths $L_{\mathrm{h}}/L_{\mathrm{e}}$.

C. Fine structure of the ground biexciton state photoluminescence

In spherical NCs with a hexagonal lattice structure, such as CdSe, the ground biexciton state has zero angular momen-

TABLE I. Relative probability of transitions between the ground biexciton and ground exciton states created by linear polarized light in NCs oriented under angle θ to the light polarization vector. The probabilities are given in the $KP^2/6$ units. Constants $N^-_{\mathrm{U,L}}$ are defined by Eq. (50); $N^+_{\mathrm{U,L}}$ can be found by replacement $B^-_{0,2}$ with $B^+_{0,2}$ in Eq. (50); constants $N_2^{\mathrm{U,L}}$ are defined by Eq. (51); and $N_0^{\mathrm{U,L}}=(D\mp f)/2D$.

ex\biex	0^-	$+1$	$+2$	-2	-1	0^+
$+2$	0	$\sin^2\theta$	$4\cos^2\theta$	0	0	0
-2	0	0	0	$4\cos^2\theta$	$\sin^2\theta$	0
$+1^{\mathrm{L}}$	$2N^-_{\mathrm{L}}\sin^2\theta$	$4N_0^{\mathrm{L}}\cos^2\theta$	$4N_2^{\mathrm{U}}\sin^2\theta$	0	0	$2N^+_{\mathrm{L}}\sin^2\theta$
-1^{L}	$2N^-_{\mathrm{L}}\sin^2\theta$	0	0	$4N_2^{\mathrm{U}}\sin^2\theta$	$4N_0^{\mathrm{L}}\cos^2\theta$	$2N^+_{\mathrm{L}}\sin^2\theta$
$+1^{\mathrm{U}}$	$2N^-_{\mathrm{U}}\sin^2\theta$	$4N_0^{\mathrm{U}}\cos^2\theta$	$4N_2^{\mathrm{L}}\sin^2\theta$	0	0	$2N^+_{\mathrm{U}}\sin^2\theta$
$+1^{\mathrm{U}}$	$2N^-_{\mathrm{U}}\sin^2\theta$	0	0	$4N_2^{\mathrm{L}}\sin^2\theta$	$4N_0^{\mathrm{U}}\cos^2\theta$	$2N^+_{\mathrm{U}}\sin^2\theta$
0^{U}	$4(B^-_2-B^-_0)^2\cos^2\theta$	$6\sin^2\theta$	0	0	$6\sin^2\theta$	$4(B^+_2-B^+_0)^2\cos^2\theta$
0^{L}	0	$6\sin^2\theta$	0	0	$6\sin^2\theta$	0

tum projection on the hexagonal axis. As one can see from Tables I and II, in a single NC one can observe two transitions from the biexciton ground state with the electric field of the light perpendicular to the c axis (σ polarization) and one transition in π polarization. Just for comparison, we would like to note that in spherical zinc-blende NCs, where there are only two ground exciton and two ground biexciton states, the selection rules allow only one-color stimulated emission in each polarization mode.

In an ensemble of randomly oriented NCs all three transitions can be observed simultaneously, although with very different probabilities. Figure 5(a) shows the structure of the PL line created by decay of the ground biexciton levels in a spherical hexagonal CdSe NC. Figure 5(b) shows the relative intensity of these transitions averaged over the solid angle.

D. Fine structure of the ground exciton resonant photoexcitation

By probing the excited NCs with light one creates one of the three ground biexciton substates. In spherical NCs with a hexagonal lattice structure, such as CdSe, only one transition from the ground dark exciton state to the first excited biexciton state is possible. Size dependence of this transition energy in CdSe NCs is shown in Fig. 6(a). The energy is calculated from the energy of the transition that could be observed in spherical NCs in the absence of the electron-hole exchange interaction and crystal field splitting.

All three biexciton states could be excited in spherical NCs with a hexagonal lattice structure when pulse probes the excited exciton state. The size dependence of the corresponding transition energies in CdSe NCs is shown in Fig. 6(a). The relative intensity of these transitions for an ensemble of randomly oriented NCs is shown in Fig. 6(b). Note, that in the ensemble of randomly oriented NCs all these transitions can be observed with equal probabilities for both the linear polarized or circular polarized excitation. After an exciton relaxation to the ground dark state, only one biexciton state could be excited according to the selection rules described above. The relative intensity of this transition does not depend on size and is equal to $2KP^2/3$. This shows that a study of the induced absorption line width should allow us to determine the exciton thermalization time.

IV. DISCUSSION AND COMPARISON WITH AVAILABLE EXPERIMENTAL DATA

The theory developed in this paper is based on the strong confinement approximation.[7] Numerical analyzes show[40] that

TABLE II. Relative probability of transitions between the ground biexciton and ground exciton states created by σ^+ polarized light in NCs oriented under angle θ_k to the light-propagation direction. The probabilities are given in the $KP^2/6$ units. Constants $N^-_{\mathrm{U,L}}$ are defined by Eq. (50); $N^+_{\mathrm{U,L}}$ can be obtained by replacement of $B^-_{0,2}$ with $B^+_{0,2}$ in Eq. (50); constants $N_2^{\mathrm{U,L}}$ are defined by Eq. (51); $N_0^{\mathrm{U,L}}=(D\mp f)/2D$; and $\Theta^{\pm}_k=(1\pm\cos\theta_k)^2/2$.

ex\biex	0^-	$+1$	$+2$	-2	-1	0^+
$+2$	0	Θ^-_k	$2\sin^2\theta_k$	0	0	0
-2	0	0	0	$2\sin^2\theta_k$	Θ^+_k	0
$+1^{\mathrm{L}}$	$2N^-_{\mathrm{L}}\Theta^-_k$	$2N_0^{\mathrm{L}}\sin^2\theta_k$	$4N_2^{\mathrm{U}}\Theta^+_k$	0	0	$2N^+_{\mathrm{L}}\Theta^-_k$
-1^{L}	$2N^-_{\mathrm{L}}\Theta^+_k$	0	0	$4N_2^{\mathrm{U}}\Theta^-_k$	$2N_0^{\mathrm{L}}\sin^2\theta_k$	$2N^+_{\mathrm{L}}\Theta^+_k$
$+1^{\mathrm{U}}$	$2N^-_{\mathrm{U}}\Theta^-_k$	$2N_0^{\mathrm{L}}\sin^2\theta_k$	$4N_2^{\mathrm{L}}\Theta^+_k$	0	0	$2N^+_{\mathrm{U}}\Theta^-_k$
-1^{U}	$2N^-_{\mathrm{U}}\Theta^+_k$	0	0	$4N_2^{\mathrm{L}}\Theta^-_k$	$2N_0^{\mathrm{U}}\sin^2\theta_k$	$2N^+_{\mathrm{U}}\Theta^+_k$
0^{U}	$2(B^-_2-B^-_0)^2\sin^2\theta_k$	$6\Theta^+_k$	0	0	$6\Theta^-_k$	$2(B^+_2-B^+_0)^2\sin^2\theta_k$
0^{L}	0	$6\Theta^+_k$	0	0	$6\Theta^-_k$	0

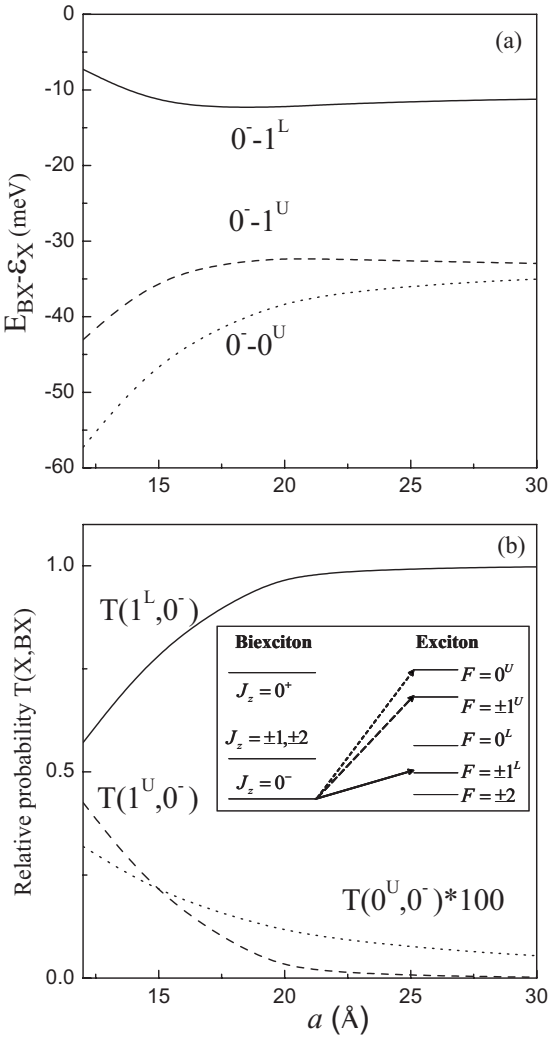

FIG. 5. (a) Size dependence of the ground biexciton state photoluminescence fine structure in spherical CdSe NCs with the standard CP and (b) the respective relative transition probabilities. Solid line corresponds to the strongest transition to the lower 1^L exciton state, dashed line—to the transition to the 1^U exciton state and dotted line—to the 0^U exciton state. The respective transition probabilities are multiplied by factor 100. The zero energy in (a) corresponds to the transition energy which would be observed in spherical NCs in the absence of the electron-hole and hole-hole exchange interaction and the crystal-field splitting. The probabilities are given in the $2KP^2/3$ units. The insert shows the schematic of the considered transitions.

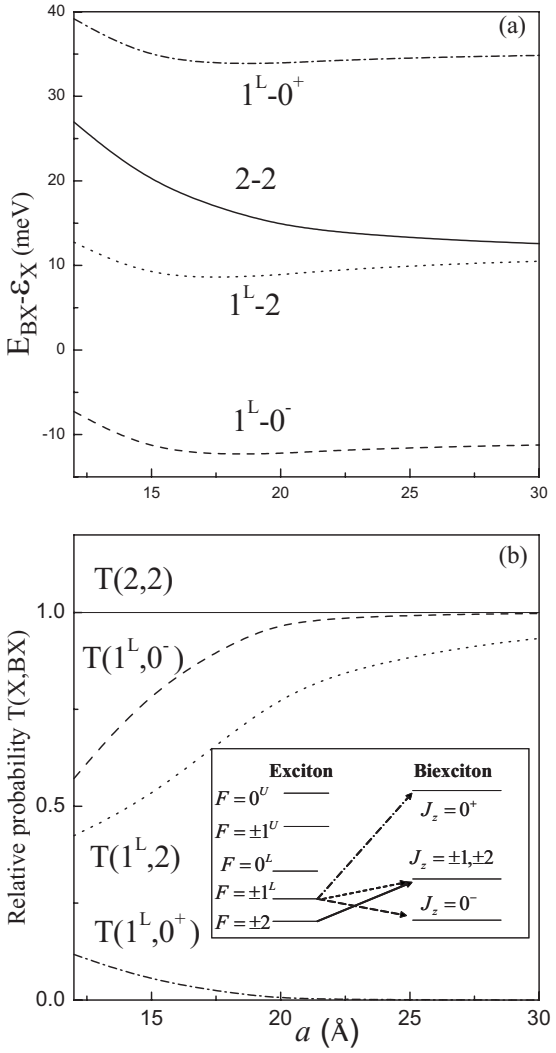

FIG. 6. (a) Size dependence of the exciton-biexciton resonant photoexcitation energy in spherical CdSe NCs with the standard CP and (b) the respective relative transition probabilities. Solid line corresponds to the excitation from the exciton ground state $|F|=2$, the dashed, dotted, and dash-dotted lines correspond to the transitions from the lowest 1^L exciton state to the 0^-, $J=2$, and 0^+ biexciton states, respectively. The zero energy corresponds to the transition energy, which would be observed in spherical NCs in the absence of the electron-hole exchange interaction and the crystal-field splitting. The probabilities are given in the $2KP^2/3$ units. The insert shows the schematic of the considered transitions.

for electrons this approximation works very well if $a \leq 3a_e$, where $a_e = \kappa\hbar^2/e^2m_e$ is the electron Bohr radius defined via the electron charge, e, the electron effective mass, m_e, and the dielectric constant, κ. For holes in the degenerate valence band, the strong confinement approximation is satisfied when $a \leq 5a_h$, where $a_h = \kappa\hbar^2/e^2m_h$ is the Bohr radius of heavy hole. We connect the numerical factors "3" and "5" in these estimates with numerical increases of confinement energy of electron and hole ground states in NCs, which for electrons and holes are described as $\approx 3^2(\hbar^2/2m_ea^2)$ and $\approx 5^2(\hbar^2/2m_ha^2)$, respectively. The developed theory can be extended, however, to the case when the condition $a \leq 5a_h$ is not satisfied because of a very large value of the heavy hole effective mass. The Coulomb potential of an electron acting on a hole in this case can be averaged out over its fast motion. This would create an additional potential for the hole motion that should be added to the confinement potential $V_h(r)$. The additional potential has a parabolic form at the NC center[7] and could be taken easily into account from calculations of the hole wave functions using the variational approach described in our paper.

The developed theory neglects also the long-range exchange contribution to the e-h exchange interaction, η, in the exciton states. Generally the contribution of the long-range

exchange interaction to the exciton energy spectra and wave functions can be described by adding some term η' to η in all equations from Eqs. (21)–(28).[41] The magnitude of η' is under discussion, however, because the effective mass approach[41] and the expansion in Wannier functions[42,43] gives different results for this value. The tight-binding approach to this problem[44] has demonstrated that the magnitude of η' depends on the relative values of the intraatomic and interatomic velocity operators. The relative values of these operators are generally unknown, resulting in a large uncertainty in the η' value. Empirically, the exciton fine structure measured in CdSe NCs in Ref. 25 was quantitatively described using $\eta'=0$ and we use the same approach in the current paper.

The multiband effective mass approach used in this paper is not valid in small NCs where the number of atoms in the NC core is smaller than those on the surface. Only an atomistic approach can fully describe energy spectra and excitations in such NCs. For the larger NCs such as were studied in Ref. 17, both the atomistic and effective mass approaches should give the same results, in principle. Differences can arise from different descriptions of the NC surface. In the multiband effective mass approximation the surface is described by additional phenomenological parameters, which may be extracted from experimental data (see, for example, Ref. 45). They also can be set to be zero, as was done in this paper and in the majority of other papers describing electronic and optical properties of CdSe NCs. The atomistic empirical pseudopotential approach in Ref. 17 used fictitious atoms to passivate the surface, which leads to different boundary conditions for the intrinsic electron and hole states in the NC.

At present there are no direct measurements of the biexciton fine structure or the fine structure of the optical transitions between exciton and biexciton states. The fine structure of the ground biexciton PL and the exciton resonant photoexcitation is difficult to observe in ensemble measurements because of the dispersion of NC sizes and shapes. These measurements require single NC studies. The pump-probe ensemble measurements, however, allow us to observe the redshift of the maximum of biexciton PL spectrum from the maximum of resonant exciton photoexcitation, known as the global Stokes shift of the biexciton PL.

The global Stokes shift of the biexciton was observed experimentally in Ref. 17. The measurements demonstrated that the shift depends on the NC's size, temperature and pump-probe delay time. At room temperatures, for the short pump-probe delay time ($\Delta t<1$ ps), the measured Stokes shift was 73 meV, 57 meV, and 45 meV in NCs with radii of $a=15$ Å, $a=21$ Å, and $a=28$ Å, respectively.

To describe the experimental results, we first calculated the biexciton Stokes shift, δ_{BX} at $T=0$ for the long pump/probe delay time ($\Delta t \gg 1$ ps). At these conditions only ground biexciton state and ground exciton states could be occupied. We obtained the values 35.9 meV, 26.9 meV, and 24.1 meV for $a=15$ Å, $a=21$ Å, and $a=28$ Å, respectively. The calculated size dependence of the biexciton Stokes shift is shown in Fig. 7 together with the experimental data and the calculated results from Ref. 17. One can see in Fig. 7 that

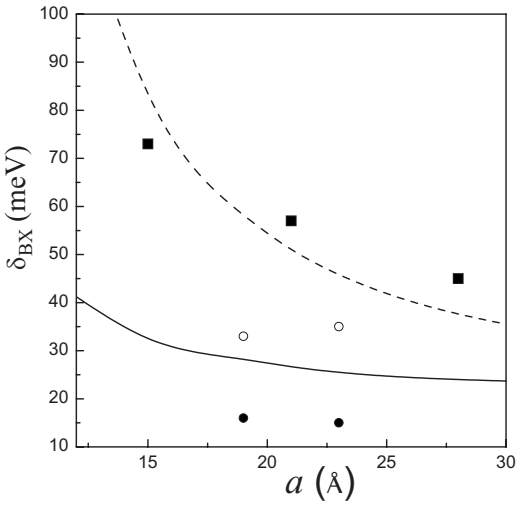

FIG. 7. Size dependence of the biexciton Stokes shift in spherical CdSe nanocrystals. The calculated dependencies for $T=0$ in spherical, with $\mu=0$, and oblate, with $\mu=-0.25$ dots are shown by solid and dashed lines, respectively. Squares show the experimental data from Ref. 17, open and black circles the calculated results from Ref. 17 for $T=0$ and $T=300$ K, respectively.

our calculations provide results very close to those calculated for two NC radii (19 and 23 Å) in Ref. 17. However, the calculations of Ref. 17 show an increase in the Stokes shift with NC size for $T=0$ (open circles in Fig. 7). Our calculations show monotonic decrease in the global biexciton Stokes shift with NC size growth for all temperatures. This is consistent with the experimental data. The difference is created by the e-h and h-h exchange interactions which are fully taken into account in our calculations and only partially in Ref. 17.

One can see in Fig. 7 that assumption of thermoequilibrium population of excitons and biexcitons ($T=300$ K data from Ref. 17) does not improve agreement between the theory and experiment. The experimental values of the Stokes shift measured at a short delay time (less than 1 ps) are significantly larger than the ones calculated assuming exciton and biexciton thermoequilibrium, which requires times much longer than 1 ps. The nonequilibrium populations of excitons and biexcitons might explain the disagreement of our theory with experimental data. Description of the Stokes shift measured at a short delay time requires, however, detailed knowledge of exciton and biexciton relaxation mechanisms, which does not exist today.

The other possible explanation of the disagreement is in our assumption about the spherical shape of the CdSe NCs used in the experiment of Ref. 17. Our theory allows us to calculate the effect of the NC nonspherical shape on the biexciton Stokes shift. We have found that the Stokes shift can be significantly larger in oblate NCs with $\mu<0$. The best description of the δ_{BX} experimental data obtained for $\mu=-0.25$ is shown in Fig. 7 by the dashed line calculated for long pump-probe delay time ($\Delta t \gg 1$ ps) at $T=0$ K.

In summary, we have developed a complete theory of the fine structure of the band-edge biexciton in NCs of zinc-blende and wurzite semiconductors with large spin-orbit

splitting of the valence band. The effect of the various confinement types and the NC shape on the biexciton spectra and optical transition energies for the resonant creation of biexcitons and biexciton photoluminescence decay were considered. The fine structure of the band-edge biexcitons calculated in this paper could be measured directly in PL and pump-probe experiments conducted in a new generation of semiconductor NCs with a suppressed rate of nonradiative Auger processes.

ACKNOWLEDGMENTS

The work was performed under RFFI under Grant No. 09-0201296-a. A.V.R. is grateful for the financial support received from the Swiss National Science Foundation. The authors thank A. A. Golovatenko, who has contributed to the variational calculations of the ground-state energy of the hole confined in the spherical parabolic potential. A.L.E. acknowledges support of the Office of Naval Research.

[1] S. Schmitt-Rink, D. A. B. Miller, and D. S. Chemla, Phys. Rev. B **35**, 8113 (1987).
[2] P. Horan and W. Blau, Phase Transit. **24**, 605 (1990).
[3] Y. Z. Hu, S. W. Koch, M. Lindberg, N. Peyghambarian, E. L. Pollock, and F. F. Abraham, Phys. Rev. Lett. **64**, 1805 (1990); Y. Z. Hu, M. Lindberg, and S. W. Koch, Phys. Rev. B **42**, 1713 (1990).
[4] Y. Z. Hu, S. W. Koch, and N. Peyghambarian, J. Lumin. **70**, 185 (1996).
[5] A. I. Ekimov and A. L. Efros, Phys. Status Solidi B **150**, 627 (1988).
[6] V. I. Klimov, A. Mikhailovsky, S. Xu, A. Malko, J. Hollingsworth, C. Leatherdale, and M. Bawendi, Science **290**, 314 (2000).
[7] Al. L. Efros and A. L. Efros, Sov. Phys. Semicond. **16**, 772 (1982).
[8] A. I. Ekimov, F. Hache, M. C. Schanne-Klein, D. Ricard, C. Flytzanis, I. A. Kudryavtsev, T. V. Yazeva, A. V. Rodina, and Al. L. Efros, J. Opt. Soc. Am. B **10**, 100 (1993).
[9] J. A. Gupta, D. D. Awschalom, X. Peng, and A. P. Alivisatos, Phys. Rev. B **59**, R10421 (1999).
[10] V. I. Klimov, A. Mihkailovsky, D. McBranch, C. Leatherdale, and M. Bawendi, Science **287**, 1011 (2000).
[11] V. I. Klimov, S. Hunsche, and H. Kurz, Phys. Rev. B **50**, 8110 (1994).
[12] S. L. Sewall, R. R. Cooney, K. E. H. Anderson, E. A. Dias, and P. Kambhampati, Phys. Rev. B **74**, 235328 (2006).
[13] S. L. Sewall, R. R. Cooney, K. E. H. Anderson, E. A. Dias, D. M. Sagar, and P. Kambhampati, J. Chem. Phys. **129**, 084701 (2008).
[14] M. Achermann, J. A. Hollingsworth, and V. I. Klimov, Phys. Rev. B **68**, 245302 (2003).
[15] J. Michel Caruge, Y. Chan, V. Sundar, H. J. Eisler, and M. G. Bawendi, Phys. Rev. B **70**, 085316 (2004).
[16] C. Bonati, M. B. Mohamed, D. Tonti, G. Zgrablic, S. Haacke, F. van Mourik, and M. Chergui, Phys. Rev. B **71**, 205317 (2005).
[17] S. L. Sewall, A. Franceschetti, R. R. Cooney, A. Zunger, and P. Kambhampati, Phys. Rev. B **80**, 081310 (2009).
[18] Al. L. Efros and A. V. Rodina, Solid State Commun. **72**, 645 (1989).
[19] X. Wang, X. Ren, K. Kahen, M. A. Hahn, M. Rajeswaran, S. Maccagnano-Zacher, J. Silcox, G. E. Cragg, Al. L. Efros, and T. D. Krauss, Nature (London) **459**, 686 (2009).
[20] P. Spinicelli, S. Buil, X. Que'lin, B. Mahler, B. Dubertret, and J.-P. Hermier, Phys. Rev. Lett. **102**, 136801 (2009).
[21] F. García-Santamaría, Y. Chen, J. Vela, R. D. Schaller, J. A. Hollingsworth, and V. I. Klimov, Nano Lett. **9**, 3482 (2009).
[22] R. Osovsky, D. Cheskis, V. Kloper, A. Sashchiuk, M. Kroner, and E. Lifshitz, Phys. Rev. Lett. **102**, 197401 (2009).
[23] L. E. Brus, J. Chem. Phys. **79**, 5566 (1983).
[24] D. J. Norris and M. G. Bawendi, Phys. Rev. B **53**, 16338 (1996).
[25] Al. L. Efros, M. Rosen, M. Kuno, M. Nirmal, D. J. Norris, and M. Bawendi, Phys. Rev. B **54**, 4843 (1996).
[26] M. Nirmal, D. J. Norris, M. Kuno, M. G. Bawendi, Al. L. Efros, and M. Rosen, Phys. Rev. Lett. **75**, 3728 (1995).
[27] D. J. Norris, Al. L. Efros, M. Rosen, and M. G. Bawendi, Phys. Rev. B **53**, 16347 (1996).
[28] S. Flügge, *Practical Quantum Mechanics I* (Springer-Verlag, Berlin, New York, 1971).
[29] G. B. Grigoryan, E. M. Kazaryan, Al. L. Efros, and T. V. Yazeva, Sov. Phys. Solid State **32**, 1031 (1990).
[30] B. L. Gel'mont and M. I. D'yakonov, Sov. Phys. Semicond. **7**, 1345 (1973).
[31] G. L. Bir and G. E. Pikus, *Symmetry and Strain-Induced Effects in Semiconductors* (Wiley, New York, 1975).
[32] A. I. Ekimov, A. A. Onushchenko, A. G. Plukhin, and Al. L. Efros, Sov. Phys. JETP **61**, 891 (1985).
[33] J. B. Xia, Phys. Rev. B **40**, 8500 (1989).
[34] Al. L. Efros, Phys. Rev. B **46**, 7448 (1992).
[35] Al. L. Efros and A. V. Rodina, Phys. Rev. B **47**, 10005 (1993).
[36] There is the misprint in Ref. 35: m_0 in Eq. (8) should be replaced by $2m_h$.
[37] R. J. Elliott, Phys. Rev. **108**, 1384 (1957).
[38] V. Berestetzkii, E. M. Lifshitz, and L. P. Pitaevskii, *Relativistic Quantum Mechanics* (1986), Vol. 4.
[39] Al. L. Efros, *Semiconductor and Metal Nanocrystals: Synthesis, Electronic and Optical Properties*, edited by V. Klimov (Pergamon, New York, 2003), Cahp. 3.
[40] A. I. Ekimov, A. A. Onushchenko, S. K. Shumilov, and Al. L. Efros, Sov. Tech. Phys. Lett. **13**, 115 (1987).
[41] S. V. Goupalov and E. L. Ivchenko, Phys. Solid State **42**, 2030 (2000).
[42] T. Takagahara, Phys. Rev. B **47**, 4569 (1993); **60**, 2638 (1999).
[43] T. Takagahara, J. Lumin. **87-89**, 308 (2000); Phys. Rev. B **62**, 16840 (2000).
[44] S. V. Goupalov and E. L. Ivchenko, Phys. Solid State **43**, 1867 (2001).
[45] J. A. Gupta, D. D. Awschalom, Al. L. Efros, and A. V. Rodina, Phys. Rev. B **66**, 125307 (2002).